International Journal of Biological and Pharmaceutical Sciences Archive

ISSN: 0799-6616 (Online)

Journal homepage: https://ijbpsa.com/

(RESEARCH ARTICLE)

Check for updates

COMPUTATIONAL PRIORITIZATION OF NOVEL NABUMETONE-DERIVED HETEROCYCLES AS POTENTIAL CYCLOOXYGENASE-2 INHIBITORS

Asmaa Adnan Abdulnabi [1,*] and Shireen Nadhem Saleh [2]

[1] College of Pharmacy, Al-Nahrain University, Baghdad, Iraq.
[2] College of Pharmacy, Tikrit University, Iraq.
* Corresponding Author; Email: asmaa.adnan@nahrainuniv.edu.iq

ORCID Details
Asmaa Adnan Abdulnabi: https://orcid.org/0000-0002-0503-0298
Shireen Nadhem Saleh: https://orcid.org/0009-0003-6623-4467

International Journal of Biological and Pharmaceutical Sciences Archive, 2026, 12(01), 192–207

Publication history: Received on 27 July 2026; revised on 07 September 2026; accepted on 09 September 2026

Article DOI: https://doi.org/10.53771/ijbpsa.2026.12.1.0087

ABSTRACT

Purpose: To prioritize fifteen novel nabumetone-derived heterocycles as potential cyclooxygenase-2 inhibitors using an integrated in silico workflow.

Methods: Compounds N1-N15 were evaluated by molecular docking against meloxicam-bound murine cyclooxygenase-2 (PDB ID: 4M11) using MOE 2019. The protocol was validated by meloxicam re-docking. The highest-ranked compound, N9, was further examined using a 100-ns GROMACS molecular dynamics trajectory. SwissADME and ADMETlab 3.0 were used for drug-likeness, pharmacokinetic and toxicity prediction.

Results: Meloxicam scored -7.256 kcal/mol, whereas all designed compounds produced more negative docking scores. N9 ranked first (-9.636 kcal/mol), followed by N14 and N13. Its predicted pose involved Tyr355 and Val116 hydrogen bonds with additional hydrophobic contacts. During the molecular dynamics trajectory, protein and ligand motion became bounded after the initial relaxation period, while compactness and persistent contacts were maintained. N9 showed high predicted gastrointestinal absorption, no blood-brain barrier permeation and no Lipinski violations. However, toxicity prediction indicated potential safety liabilities, including drug-induced liver injury, genotoxicity and neurotoxicity.

Conclusions: N9 is the top candidate in this computational series and should be synthesized and tested for cyclooxygenase inhibition, anti-inflammatory activity and safety.

Keywords: Cyclooxygenase-2, ADMET, Molecular docking, Molecular dynamics, Nabumetone derivatives

1 INTRODUCTION

Inflammation is a normal protective response to tissue injury, infection, and other harmful stimuli. It is resolved under healthy conditions after the initial threat is controlled. However, if inflammatory signaling continues, the response may be harmful and lead to chronic tissue damage in multiple organ systems [1]. Lipid mediators such as prostaglandins play a crucial role in this process. They are produced from arachidonic acid by the cyclooxygenase pathway and play a role in the regulation of vascular tone, tissue permeability, pain sensitization, fever and leukocyte behaviour. The pathway connecting normal homeostasis and inflammatory signaling makes cyclooxygenase enzymes important targets for pharmacologic intervention [2]. Cyclooxygenase-1 (COX-1) and cyclooxygenase-2 (COX-2) catalyze closely related reactions, but are expressed differently. COX-1 is widely distributed and participates in many processes, such as protection of the mucosa in the stomach and platelet activation, whereas COX-2 is very sensitive to inflammatory and mitogenic stimuli. This difference was the foundation for the creation of agents targeted at blocking the production of pathological prostaglandins with minimal impact on normal COX-1 activity [3,4]. Non-steroidal anti-inflammatory drugs (NSAIDs) are commonly prescribed for pain and inflammation, but have known gastrointestinal, renal, and cardiovascular side effects. COX-2 selective agents were found to be more tolerable in the gastrointestinal tract in many patients, but later cardiovascular issues revealed that selectivity is not sufficient to ensure an optimal therapeutic profile. Thus, research into drug discovery is ongoing to find a balance between activity, selectivity, and safety [5].

Medicinal-chemistry research in this area has focused on COX-2-directed scaffolds, substitutions and heterocyclic systems. The goal is to maintain the productive ligand interactions in the cyclooxygenase channel with the enhancement of selectivity and physicochemical properties. Recent research on pyrazole-based inhibitors and on other recently described COX-2-directed compounds demonstrates that relatively small structural modifications can have significant effects on affinity, selectivity and anti-inflammatory activity [6,7]. An alternative is to modify existing NSAID structures, instead of starting from scratch with a different chemotype. This approach has recently been applied to find safer COX-2 inhibitors and to modify existing scaffolds such as indoprofen to yield more COX-2 selective compounds [8]. The scaffold-remodeling approach has been used for fenamates and ibuprofen, and indole-containing systems offer another proven pathway to COX-2-directed design. In these methods, the parent pharmacophore is a known structure and the new groups are added to increase the interaction pattern into other parts of the binding pocket [9,10].

Heterocycles are especially valuable in this context because they can change the polarity, geometry, hydrogen-bonding ability, aromatic recognition, and conformational properties of the parent scaffold. They are important because there are many drugs approved that have rings with nitrogen, oxygen, or sulfur. Nabumetone is appropriate for this kind of structural elaboration and recent efforts in the design of nabumetone-linked pyrazole and thiadiazole derivatives justify further investigation of this scaffold for anti-inflammatory design [11,12].

In recent years, in silico studies have been performed to assess and prioritize newly designed drug candidates for experimental validation by using molecular docking, molecular dynamics and ADME profiling [13,14]. Docking can propose reasonable binding orientations in a specific receptor model, and molecular dynamics (MD) can simulate the dynamics of a chosen complex over time.

2 MATERIALS AND METHODS

2.1 Computational workflow

The fifteen compounds (N1-N15) were screened according to the workflow presented in Figure 1. The workflow included ligand and receptor preparation, meloxicam re-docking, comparative docking of the full series, selection of the highest-ranked compound N9, analysis of a 100-ns GROMACS trajectory of the N9-COX-2 complex, SwissADME screening, and ADMETlab 3.0 toxicity prediction. The individual outputs were considered together for computational prioritization and require experimental confirmation.

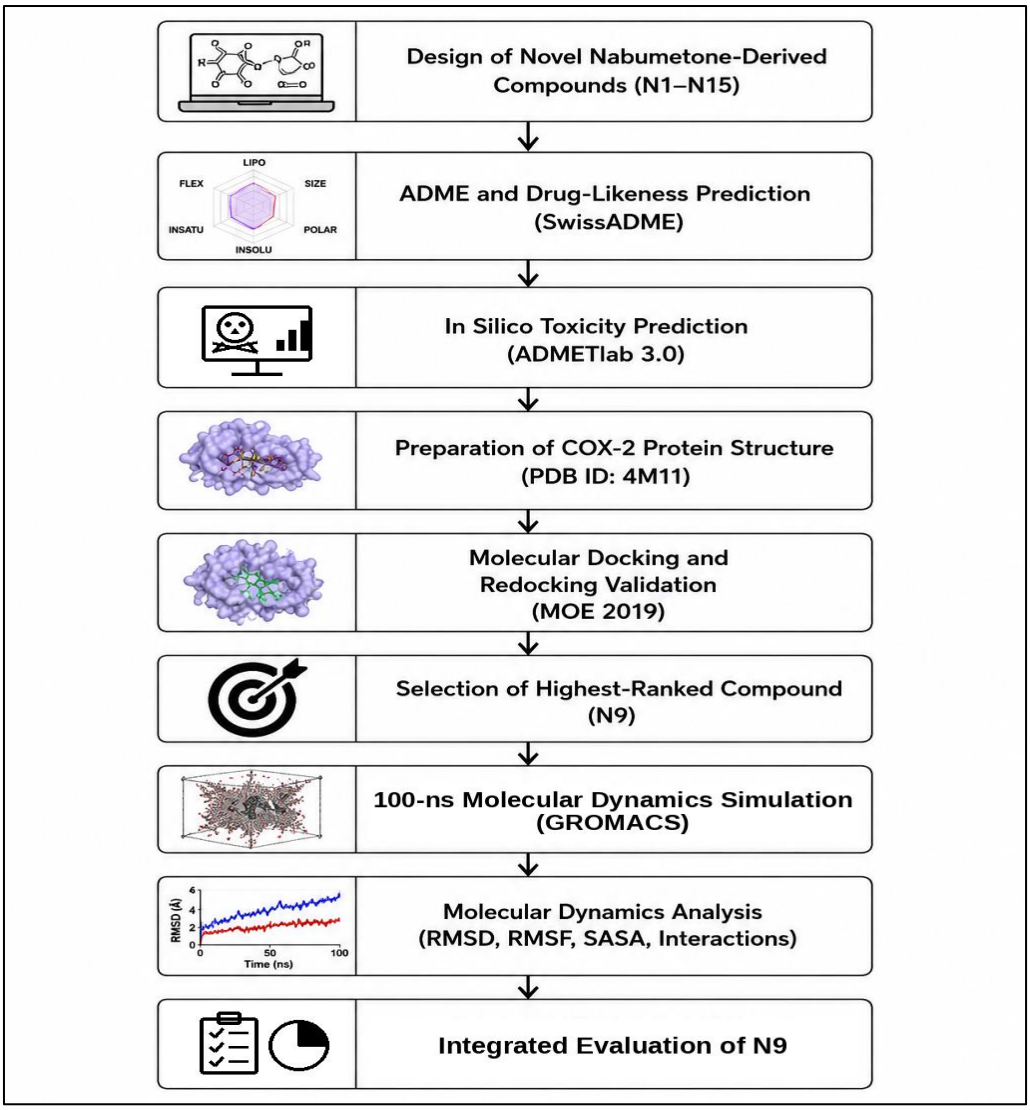

Figure 1: Computational workflow for evaluating N1-N15

2.2 Protein and ligand preparation

The meloxicam-bound X-ray structure of murine COX-2 (Protein Data Bank (PDB) ID: 4M11; 2.45 Å resolution) was selected because it provides an experimentally defined ligand pose for both pocket identification and docking validation [15].

Chain A was kept. The receptor was prepared using the Molecular Operating Environment (MOE 2019) Structure Preparation and Protonate3D tools after removing heme components, crystallographic waters, and non-essential heteroatoms following the docking protocol. The crystallographic water treatment is explicitly mentioned as the native meloxicam complex contains ordered water mediated contacts. The 15 ligands were created in chemically reasonable low energy conformations and minimized prior to docking.

2.3 Molecular docking and validation

Every derivative was tested in the same experimentally defined pocket [16] centered on the co-crystallized meloxicam. Meloxicam was removed and re-docked as an internal validation. The crystallographic orientation was reproduced with the best pose differing by 1.35 Å, which was a good agreement. The protocol was then validated and applied to N1-N15 without changes, and the top-ranked pose for each compound was kept for interaction analysis. MOE scores were only used for ranking compounds within this protocol and were not considered to be experimental binding free energies or direct estimates of IC50 or Ki.

2.4 Molecular dynamics simulation and trajectory analysis

N9 was selected for molecular dynamics because it produced the most negative docking score. The differences from N14 and N13 were small, however, at only 0.14 and 0.23 kcal/mol, respectively. N9 is therefore described as the highest-

ranked compound rather than as a definitively superior member of the series. A single 100-ns all-atom production trajectory of the N9-COX-2 complex generated with GROMACS [17] was analyzed using protein Cα root-mean-square deviation, ligand root-mean-square deviation after protein fitting, radius of gyration, solvent-accessible surface area, ligand per-atom root-mean-square fluctuation, and protein-ligand contact profiles and occupancies. Because only one production trajectory was analyzed, these results are interpreted as supportive evidence of dynamic stability, not as proof of convergence, uninterrupted ligand residence, or binding affinity. Residue numbering in the trajectory-analysis output differs from standard 4M11 numbering; the relevant correspondences are Arg89/Arg120, Val85/Val116, Tyr324/Tyr355, Ile314/Ile345, Met82/Met113, Glu493/Glu524, Ser499/Ser530, Arg482/Arg513, and Leu500/Leu531.

2.5 ADME and drug-likeness prediction

SwissADME was used to estimate physicochemical, absorption-related, and medicinal-chemistry properties for N1-N15 [18]. The recorded descriptors included molecular weight, topological polar surface area, consensus Log P, predicted gastrointestinal absorption, predicted blood-brain barrier permeation, P-glycoprotein substrate status, Lipinski compliance, bioavailability score, ESOL class, pan-assay interference compound alerts, Brenk alerts, and synthetic accessibility. These values were treated as model-based estimates. The BOILED-Egg model was chosen for its graphical representation of predicted passive gastrointestinal absorption and brain permeation as a summary, but not as proof of measured pharmacokinetics or safety [19].

2.6 In silico toxicity prediction

In silico toxicity profiles for N1-N15 were evaluated with ADMETlab 3.0 [20]. The assessed endpoints included human ether-à-go-go-related gene channel blockade, drug-induced liver injury, Ames mutagenicity, carcinogenicity, skin sensitization, human hepatotoxicity, drug-induced nephrotoxicity, drug-induced neurotoxicity, genotoxicity, and other toxicity-related outputs available from the platform. Probability scores were interpreted as screening signals rather than experimental toxicity measurements, with higher values indicating a higher model-predicted probability for the corresponding endpoint.

3 RESULTS

3.1 Molecular docking

The MOE docking scores, key predicted interactions, and chemical structures of N1-N15 are summarized in Table 1. Under the same protocol, meloxicam scored -7.256 kcal/mol, while the designed compounds ranged from -7.701 to -9.636 kcal/mol. N9 ranked first, followed by N14, N13, N12, and N7. These scores are presented for relative comparison within this docking setup and should not be interpreted as experimental binding free energies.

Table 1: Docking scores, key COX-2 interactions, and chemical structures of N1-N15

Compound	Docking score (kcal/mol)	Key binding interactions (residues and distances, Å)	Structure
N1	-7.770	H-bond: Met535 (3.57 Å); C-H: Tyr385; hydrophobic: Ala527, Leu352, Trp387, Val523, Val349, Arg120.	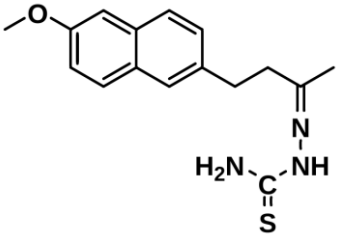
N2	-7.701	H-bond: Arg120 (3.04 Å); C-H: Met522; hydrophobic: Phe518, Ala527, Val349, Trp387, Val523.	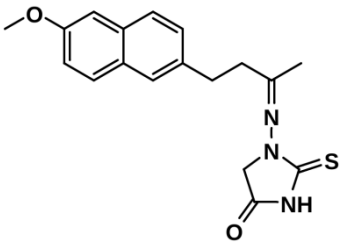

N3	-8.530	Amide-π: Gly526; hydrophobic: Tyr385, Trp387, Phe381, Val523, Leu384, Ala527.	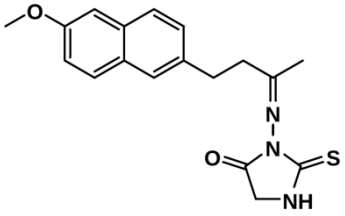
N4	-8.341	H-bonds: Arg120 (2.32, 2.36 Å), Ser119 (3.11 Å), Val116 (3.43, 3.70 Å); C-H: Tyr355; hydrophobic: Met522, Phe518, Trp387, Ala527.	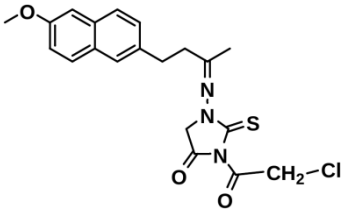
N5	-8.484	Halogen bond (Cl): Ala527; amide-π: Gly526; C-H: Ser530; hydrophobic: Met522, Leu117, Trp387.	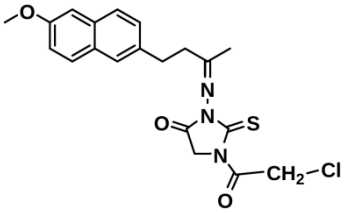
N6	-8.455	C-H: Met522; hydrophobic: Leu352, Val523, Val349, Ala527, Ile345, Phe518, Trp387.	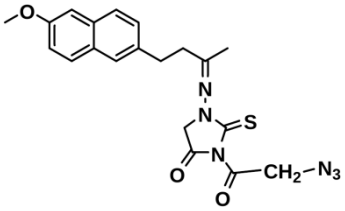
N7	-9.069	Amide-π: Gly526; hydrophobic: Arg120, Phe381, Trp387, Tyr385, Leu384, Ala527.	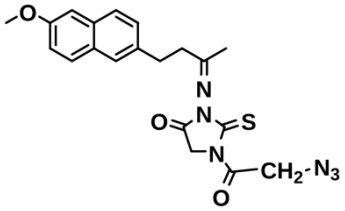
N8	-8.872	H-bonds: Arg120 (2.41 Å), Ser119 (2.94 Å), Val116 (3.52, 3.75 Å); π-donor: Tyr115; amide-π: Gly526; hydrophobic: Ala527, Phe518, Trp387.	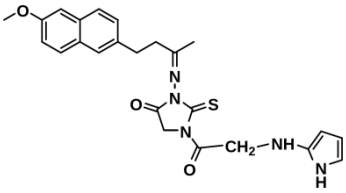
N9	-9.636	H-bonds: Tyr355 (3.07 Å), Val116 (3.06 Å); hydrophobic: Arg120, Val523, Leu352, Phe518, Ala527, Ile345, Met535.	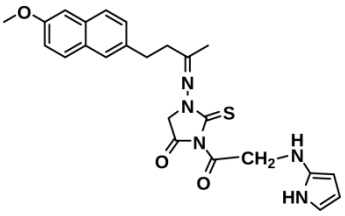
N10	-8.497	H-bonds: Ser530 (2.31, 2.99 Å), Ala527 (3.26 Å); amide-π: Gly526; π-donor: Tyr115; hydrophobic: Arg120, Val116, Tyr355.	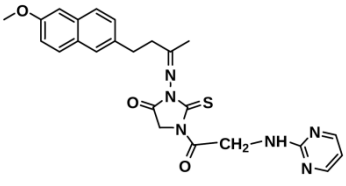

N11	-8.624	H-bonds: Arg120 (2.14 Å), Ser119 (2.28, 2.81 Å), Val116 (3.04 Å); attractive charge/π-cation: Glu524, Arg120; hydrophobic: Met522, Phe518, Trp387.	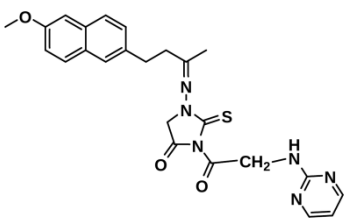
N12	-9.112	H-bond: Tyr355 (3.32 Å); π-cation: Arg120 (3.33, 3.55 Å); C-H: Glu524, Ala527; π-sulfur: Met535; amide-π: Ser530.	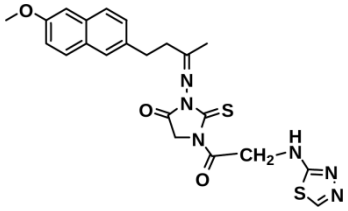
N13	-9.406	π-cation: Arg120 (3.15 Å); C-H: Glu524, Pro86; amide-π: Gly526; hydrophobic: Phe518, Trp387.	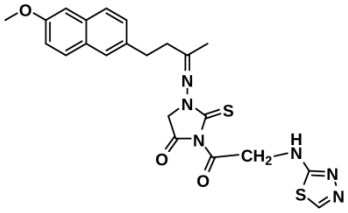
N14	-9.496	H-bond: Tyr355 (3.54 Å); π-cation: Arg120 (3.24, 3.41 Å); C-H: Ala527; π-sulfur: Met535; hydrophobic: Ile345, Leu531.	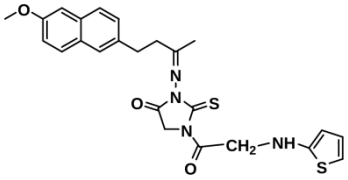
N15	-8.977	H-bonds: Arg120 (3.00 Å), Tyr385 (3.00 Å); C-H: Ser119, Pro86, Gly526; π-sulfur: Met113; hydrophobic: Leu93, Val349, Ala527.	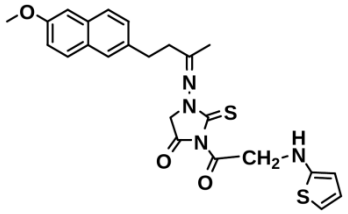

The predicted N9 pose formed hydrogen bonds with Tyr355 (3.07 Å) and Val116 (3.06 Å), while Arg120, Val523, Leu352, Phe518, Ala527, Ile345, and Met535 contributed hydrophobic contacts (Table 1). N14 retained a Tyr355 hydrogen bond together with π-cation contacts involving Arg120. N13 combined a π-cation interaction with Arg120 with amide-π and hydrophobic contacts, whereas N12 paired a Tyr355 hydrogen bond and Arg120 π-cation contacts with C-H, π-sulfur, and amide-π interactions. Figure 2 summarizes the docking interactions of meloxicam and the five highest-ranked designed compounds.

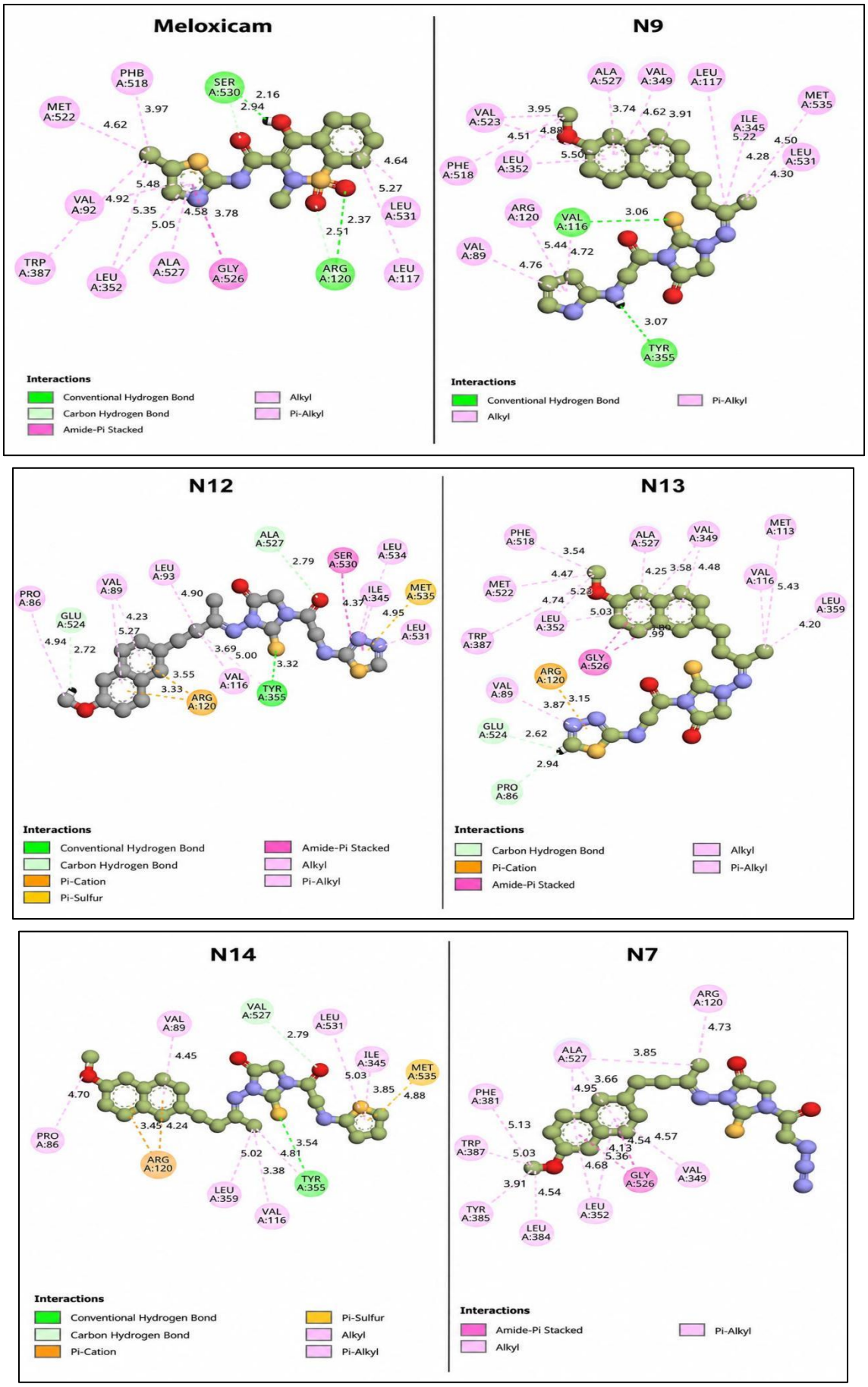

Figure 2: Docking interactions of meloxicam and selected top-ranked compounds: (A) meloxicam, (B) N9, (C) N12, (D) N13, (E) N14, and (F) N7

N9 was therefore identified as the highest-ranked compound in the docking screen. Because its score differed from that of N14 by only 0.14 kcal/mol, the result is better used for prioritization than as evidence of a meaningful difference in affinity. N9 was consequently selected for analysis of the 100-ns GROMACS trajectory.

3.2 Molecular dynamics

3.2.1 Protein and ligand root-mean-square deviation (RMSD)

As shown in Figure 3, the COX-2 Cα RMSD increased during the initial relaxation phase and then entered a bounded regime. For most of the remaining trajectory, it stayed near 2.0-2.7 Å, apart from a brief excursion around 75 ns. N9 showed a similar overall pattern, with its RMSD remaining at approximately 4.5-5.2 Å after the initial phase.

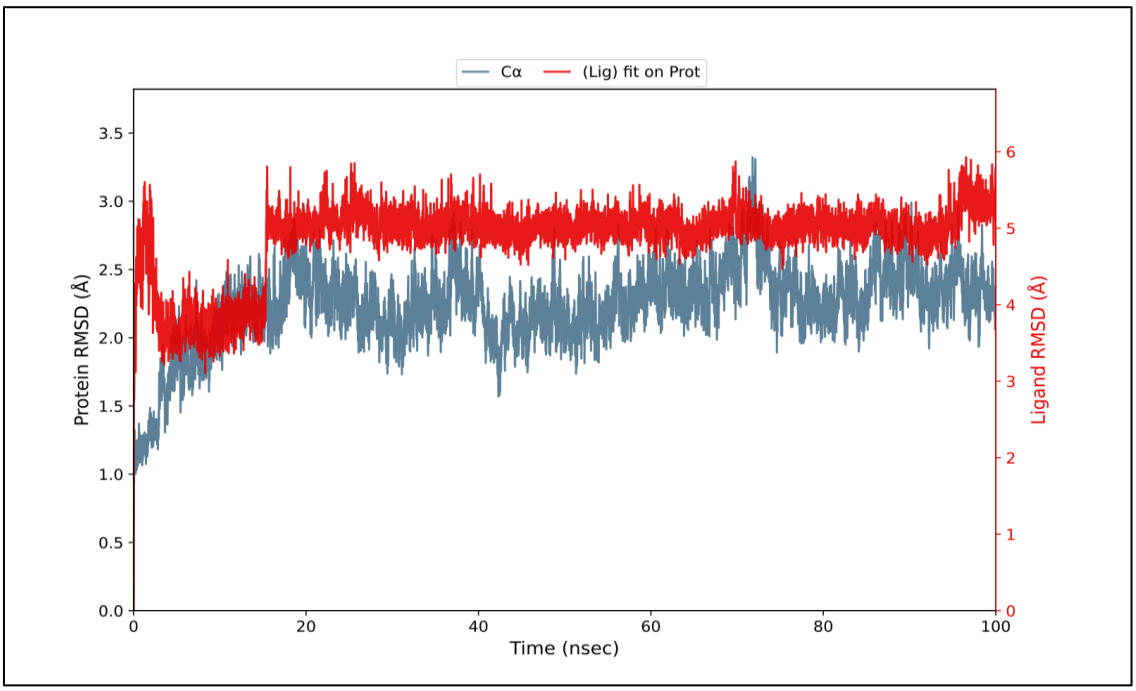

Figure 3: Protein and ligand RMSD during the 100-ns N9-COX-2 simulation

3.2.2 Ligand per-atom root-mean-square fluctuation (RMSF)

The per-atom RMSF profile of the ligand (Figure 4) revealed that the fluctuations were relatively low in most parts of the ligand, ranging from 0.7 Å to 2.8 Å. A pronounced local peak of approximately 9 Å was found at atom 16, suggesting that flexibility was focused in a small area of the ligand, rather than spread throughout the molecule.

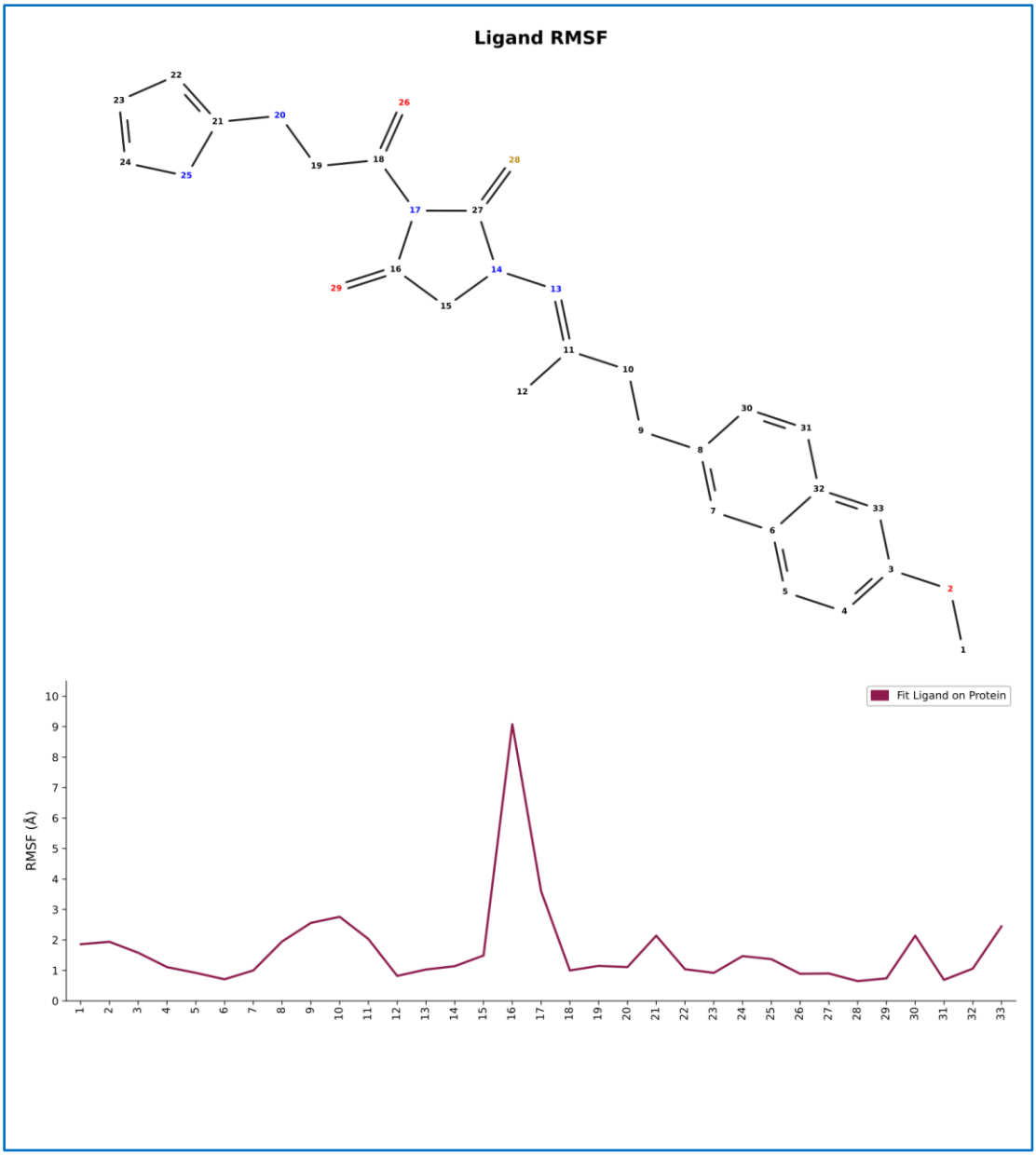

Figure 4: Ligand atom numbering and per-atom RMSF of N9 for the 100-ns simulation of N9-COX-2

3.2.3 The compactness and exposure of proteins

The radius of gyration profile is presented in Figure 5 and the solvent-accessible surface area profile is presented in Figure 6. The radius of gyration was tightly clustered around 24.6-24.9 Å during the initial relaxation period, and then only slightly reduced towards the end of the trajectory, whereas the solvent-accessible surface area was generally around 25,000-26,000 $Å^2$ and only slightly reduced later in the trajectory.

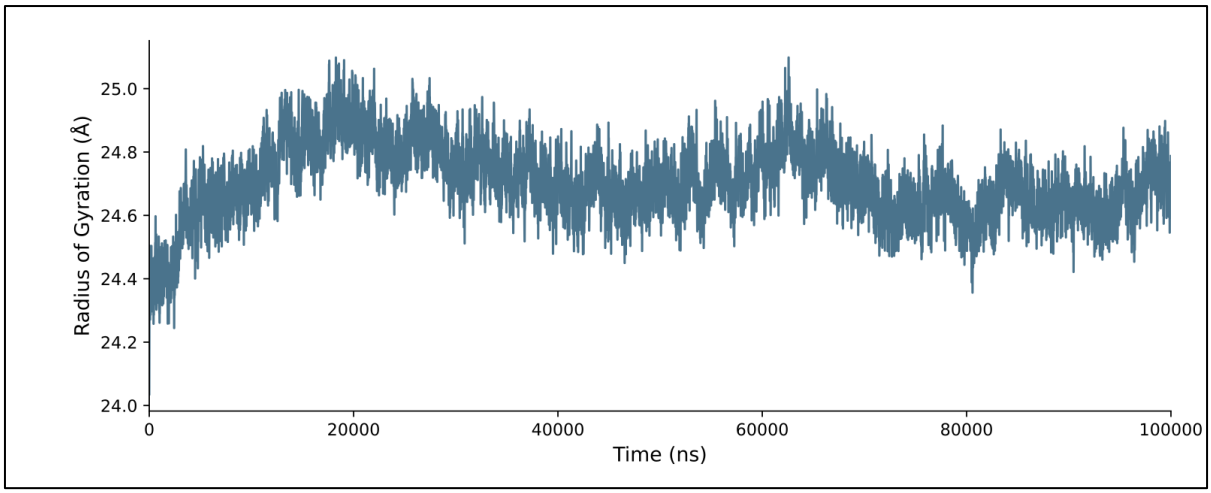

Figure 5: Radius of gyration of the N9-COX-2 complex during the 100-ns simulation

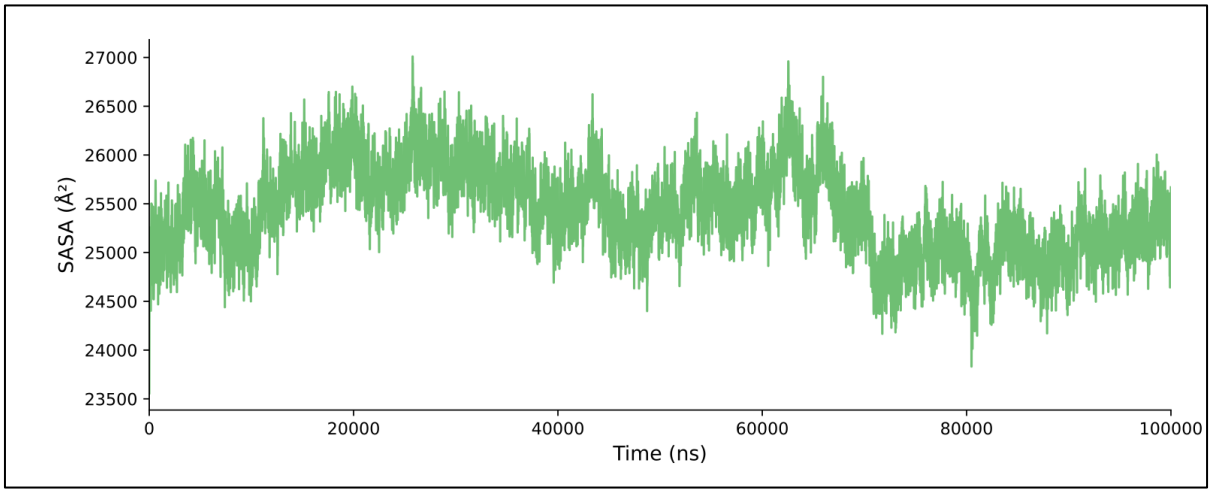

Figure 6: SASA profile of the N9-COX-2 complex during the 100-ns simulation

3.2.4 Protein-ligand contact profile and interaction persistence

The protein-ligand contact profile in Figure 7 reveals that the N9-COX-2 interaction network was primarily hydrophobic, and included ionic, direct hydrogen-bond and water-mediated contacts. For this analysis, the numbering of the residues is done along the trajectory output and is not the same as the standard 4M11 numbering.

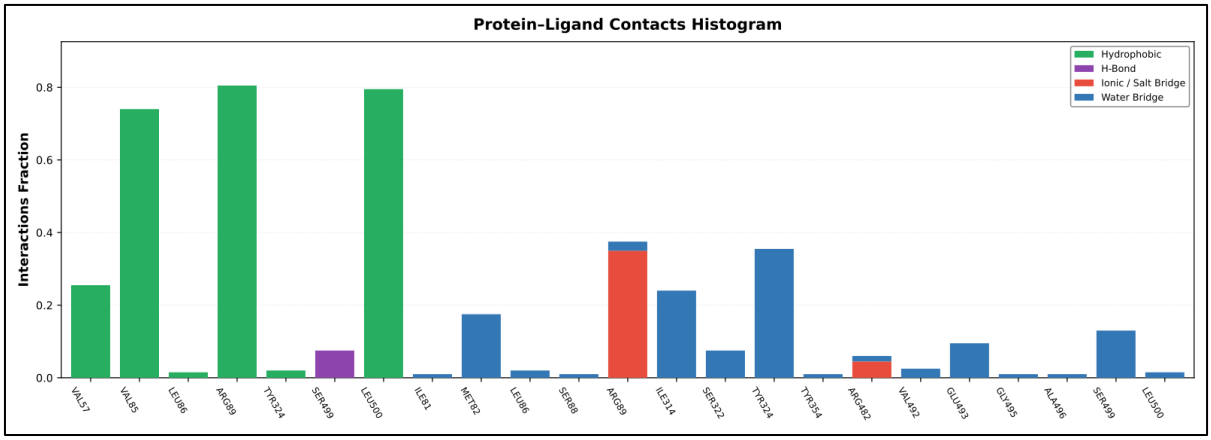

Figure 7: Protein-ligand contact profile for the N9-COX-2 complex

The two dimensional occupancy map shown in Figure 8 illustrates the occupancy of individual contacts along the 100-ns trajectory. The most common contact was Arg89, which occurred in approximately 76% of the simulation and provided an additional ionic interaction in approximately 30% of the simulation.

Leu500 and Val85 were present for approximately 58% and 54%, respectively, whereas Val57 was less persistent. Tyr324, Ile314, and Met82 contributed mainly through water-mediated contacts. In standard 4M11 numbering, Arg89 corresponds to Arg120, Leu500 to Leu531, and Val85 to Val116. Overall, the interaction pattern was distributed and adaptable rather than dependent on a single permanent hydrogen bond.

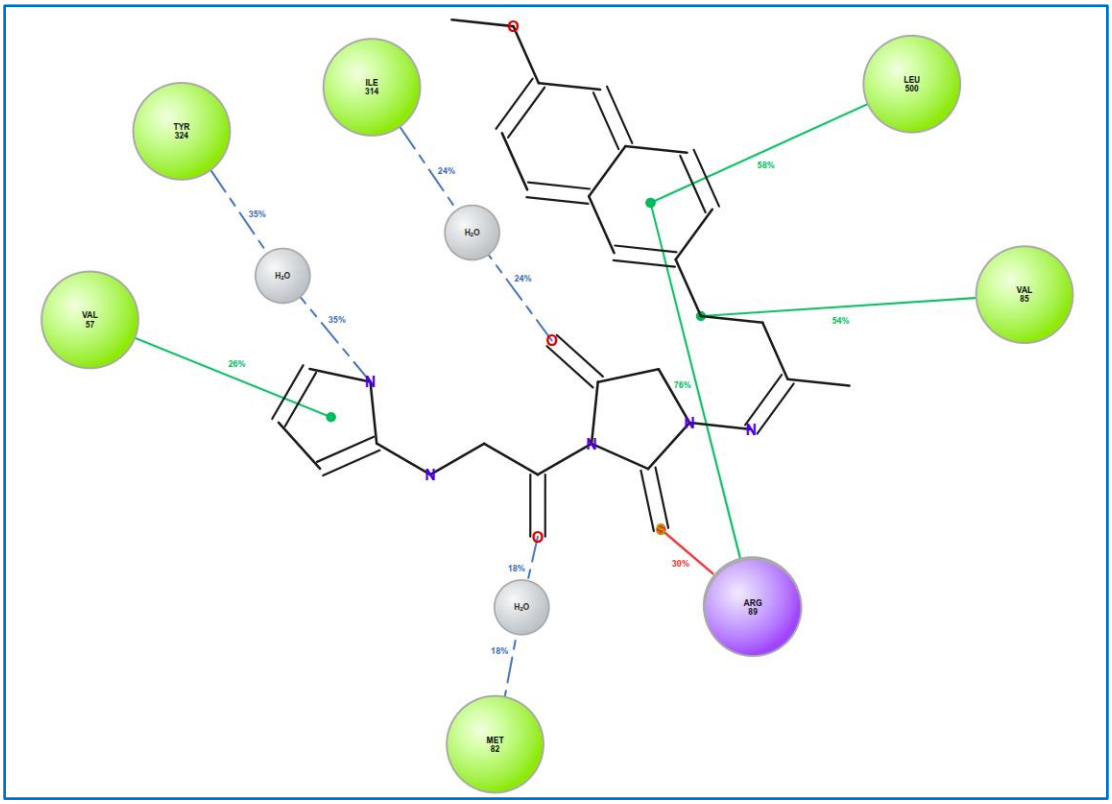

Figure 8: N9-COX-2 interaction occupancies during the 100-ns simulation

3.3 ADME and drug-likeness

SwissADME was used to compare predicted physicochemical, absorption-related, and medicinal-chemistry properties across N1-N15. The main descriptors are summarized in Table 2. All compounds had molecular weights below 500 g/mol and no predicted Lipinski violations. Consensus Log P values remained moderate across the series, whereas topological polar surface area varied more widely and broadly followed the predicted gastrointestinal-absorption classification.

Table 2: Predicted physicochemical and drug-likeness properties of N1-N15 (SwissADME)

Compound	MW (g/mol)	TPSA (Å^2)	Consensus Log P	GI absorption	BBB permeant	Lipinski violations	Bioavailability score
N1	301.41	91.73	3.13	High	No	0	0.55
N2	341.43	86.02	2.94	High	No	0	0.55
N3	341.43	86.02	2.89	High	No	0	0.55
N4	417.91	94.30	3.31	High	No	0	0.55
N5	417.91	94.30	3.14	High	No	0	0.55
N6	424.48	144.05	2.90	Low	No	0	0.55
N7	424.48	144.05	2.69	Low	No	0	0.55
N8	463.55	122.12	3.04	High	No	0	0.55
N9	463.55	122.12	3.19	High	No	0	0.55
N10	476.55	132.11	2.67	High	No	0	0.55

N11	476.55	132.11	2.81	High	No	0	0.55
N12	482.58	160.35	2.78	Low	No	0	0.55
N13	482.58	160.35	2.96	Low	No	0	0.55
N14	480.60	134.57	3.82	Low	No	0	0.55
N15	480.60	134.57	3.86	Low	No	0	0.55

As summarized in Table 2, the absorption predictions separated the series into two broad groups. N1-N5 and N8-N11 were classified as having high predicted gastrointestinal absorption, whereas N6, N7, and N12-N15 were classified as low. None of the compounds was predicted to cross the blood-brain barrier, and all had a predicted bioavailability score of 0.55. For N9, the predicted profile included a molecular weight of 463.55 g/mol, a topological polar surface area of 122.12 Å^2, a consensus Log P of 3.19, high gastrointestinal absorption, no predicted brain permeation, and no Lipinski violations. The values reflect a computational profile, not pharmacokinetics. The BOILED-Egg plot was used to visually summarize these physicochemical trends (Figure 9).

None of the compounds entered the region associated with probable blood-brain barrier permeation, whereas compounds with high predicted gastrointestinal absorption clustered in the white region. The series was also classified as predicted non-substrates of P-glycoprotein. Because the model is driven mainly by lipophilicity and polarity, the plot should be used as a screening aid rather than as evidence of measured absorption, brain exclusion, or safety. Complementary solubility and medicinal-chemistry descriptors are listed in Table 3.

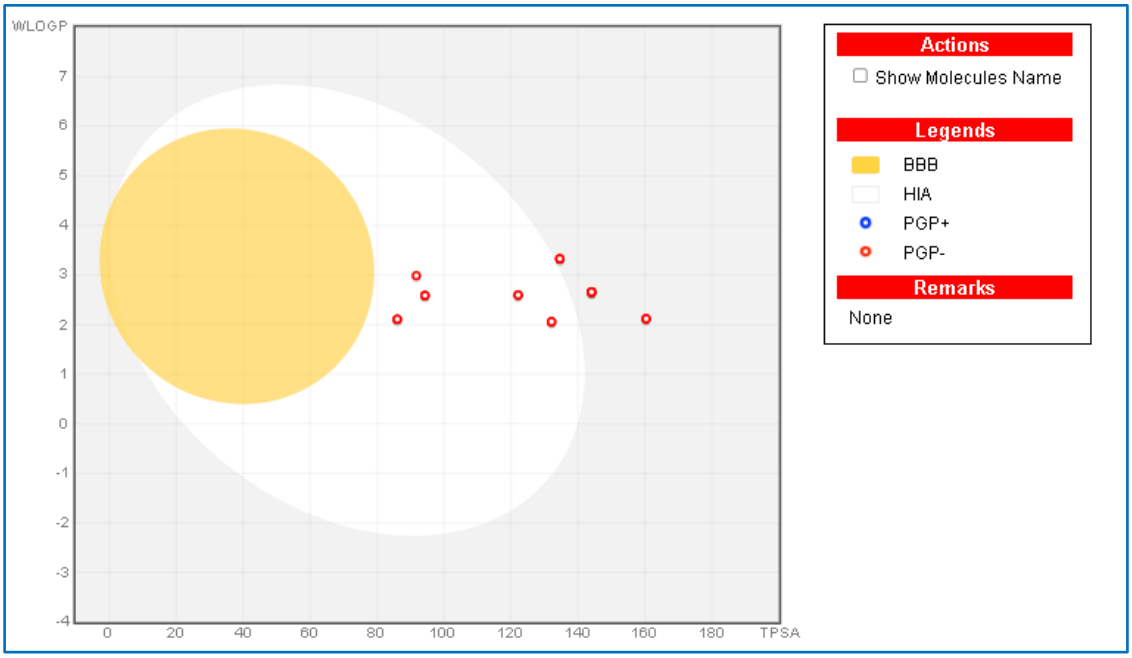

Figure 9: BOILED-Egg plot for N1-N15

Table 3: Predicted solubility and medicinal-chemistry properties of N1-N15 (SwissADME)

Compound	ESOL class	P-gp substrate	PAINS alerts	Brenk alerts	Synthetic accessibility
N1	Soluble	No	0	2	2.70
N2	Soluble	No	0	2	3.23
N3	Soluble	No	0	2	3.17
N4	Moderately soluble	No	0	3	3.56
N5	Moderately soluble	No	0	3	3.67
N6	Moderately soluble	No	1	5	3.66
N7	Moderately soluble	No	1	5	3.63

N8	Moderately soluble	No	0	2	3.81
N9	Moderately soluble	No	0	2	3.82
N10	Moderately soluble	No	0	2	3.79
N11	Moderately soluble	No	0	2	3.80
N12	Moderately soluble	No	0	2	4.01
N13	Moderately soluble	No	0	2	4.02
N14	Moderately soluble	No	0	2	3.93
N15	Moderately soluble	No	0	2	3.94

As shown in Table 3, N1-N3 were classified as soluble by the ESOL model, whereas N4-N15 were classified as moderately soluble. None of the compounds was predicted to be a P-glycoprotein substrate. PAINS alerts were absent from most of the series, with one alert each for N6 and N7. Brenk alerts ranged from two to five, and predicted synthetic-accessibility scores ranged from 2.70 to 4.02. N9 was predicted to be moderately soluble, non-P-glycoprotein, free of PAINS alerts, and associated with two Brenk alerts and a synthetic-accessibility score of 3.82.

3.4 Toxicity prediction

To complement the absorption and drug-likeness assessment, ADMETlab 3.0 toxicity predictions were evaluated for N1-N15 [20]. Selected endpoints and probability scores are summarized in Table 4. The values range from 0 to 1 and represent model-predicted probabilities rather than measured toxicities. They were used to identify potential safety liabilities that could influence prioritization and guide later experimental testing.

Table 4: Selected ADMETlab 3.0 toxicity predictions for N1-N15

Compound	hERG	DILI	AMES	Carcinog.	Genotox.	Skin sensit.	Hepatotox.	Nephrotox.	Neurotox.
N1	0.236	0.961	0.899	0.866	0.904	0.757	0.699	0.830	0.716
N2	0.128	0.994	0.904	0.929	0.995	0.942	0.769	0.794	0.771
N3	0.128	0.987	0.921	0.931	0.999	0.893	0.733	0.708	0.843
N4	0.048	0.979	0.976	0.918	1.000	0.984	0.570	0.903	0.883
N5	0.048	0.980	0.981	0.906	1.000	0.996	0.502	0.929	0.778
N6	0.073	1.000	1.000	1.000	1.000	1.000	0.963	1.000	1.000
N7	0.073	1.000	1.000	1.000	1.000	1.000	0.968	1.000	1.000
N8	0.133	0.997	0.786	0.764	1.000	0.658	0.756	0.782	0.892
N9	0.160	0.997	0.767	0.756	1.000	0.723	0.734	0.759	0.945
N10	0.323	0.996	0.563	0.906	1.000	0.888	0.729	0.907	0.846
N11	0.352	0.996	0.526	0.897	1.000	0.920	0.710	0.899	0.926
N12	0.171	1.000	0.889	0.926	1.000	0.794	0.875	0.931	0.708
N13	0.183	1.000	0.877	0.926	1.000	0.810	0.869	0.923	0.833
N14	0.249	1.000	0.900	0.867	1.000	0.744	0.837	0.867	0.719
N15	0.277	1.000	0.891	0.869	1.000	0.745	0.818	0.863	0.843

For N9, Table 4 shows a comparatively low primary hERG-blocker probability (0.160), whereas stronger model signals were predicted for drug-induced liver injury (0.997), Ames mutagenicity (0.767), carcinogenicity (0.756), genotoxicity (1.000), skin sensitization (0.723), hepatotoxicity (0.734), nephrotoxicity (0.759), and neurotoxicity (0.945).

4 DISCUSSION

Docking placed N9 at the top of the series, although its 0.14 kcal/mol difference from N14 is too small to support a firm claim of superior affinity. The predicted N9 contacts with Arg120, Tyr355 and Val116 lie within the meloxicam-defined COX-2 pocket and provide a structural rationale for its ranking [15]. Because docking scores depend on the selected protocol and scoring function, they are more appropriate for prioritization than for direct estimation of binding free energy [16].

The 100-ns trajectory added a dynamic layer to the docking result. After the initial relaxation period, protein RMSD, ligand RMSD, radius of gyration and solvent-accessible surface area remained within bounded ranges. The ligand RMSF profile showed mostly low-to-moderate local fluctuations with one pronounced flexible region, while hydrophobic, ionic and polar contacts persisted across the trajectory. This behavior supports a stable simulated N9-COX-2 complex. However, a single production trajectory cannot demonstrate convergence, residence time or biochemical potency, and replicate simulations or experimental enzyme assays would provide stronger validation.

The predicted pharmacokinetic profile of N9 was generally favorable at the screening stage, with high gastrointestinal absorption, no predicted blood-brain barrier permeation and no Lipinski violations [18,19]. Moderate solubility and two Brenk alerts remain relevant considerations. More importantly, ADMETlab 3.0 identified high-probability signals for drug-induced liver injury, genotoxicity and neurotoxicity [20]. These outputs are model predictions rather than measured toxicities, but they indicate that safety optimization should accompany any further development of N9.

Taken together, the integrated workflow narrows the fifteen novel nabumetone-derived heterocycles to N9 as the first candidate for synthesis and biological testing. The present findings support prioritization, not established anti-inflammatory activity. Biochemical COX-2/COX-1 inhibition and selectivity assays, cellular anti-inflammatory studies, experimental pharmacokinetic testing and toxicological evaluation are needed before stronger conclusions can be drawn.

5 CONCLUSION

Among the fifteen novel nabumetone-derived heterocycles evaluated in silico, N9 was the highest-ranked candidate against murine COX-2. Its docking score, 100-ns molecular dynamics behavior and predicted drug-likeness support further experimental investigation, whereas the predicted liver injury, genotoxicity and neurotoxicity signals require careful safety assessment. N9 should therefore be regarded as a prioritized computational candidate rather than a compound with established anti-inflammatory activity or safety. Synthesis, COX-2/COX-1 inhibition and selectivity assays, cellular anti-inflammatory testing, and experimental pharmacokinetic and toxicological studies are required for confirmation.

STATEMENTS ON COMPLIANCE WITH ETHICAL STANDARDS

Acknowledgments

The authors would like to thank Al-Nahrain University, College of Pharmacy and Tikrit University, College of Pharmacy for the facilities and support they provided for them to complete this research.

Disclosure of conflict of interest

No conflict of interest is associated with this work.

Use of Artificial intelligence/Large language models

The authors state that no artificial intelligence (AI) or large language models (LLMs) have been employed to prepare, write, analyse or edit this manuscript.

Use of research reporting tools

No specific EQUATOR reporting guideline was applicable to this entirely in silico study. The manuscript was prepared in accordance with the International Journal of Biological and Pharmaceutical Sciences Archive author guidelines.

Availability of data and materials

All data supporting the findings reported in this study are included in the article. Additional computational outputs are available from the corresponding author on reasonable request.

Contribution of authors

We declare that this work was done by the authors named in this article, and all liabilities pertaining to claims relating to the content of this article will be borne by the authors. Asmaa Adnan Abdulnabi and Shireen Nadhem Saleh performed the molecular docking, molecular dynamics, ADME, and toxicity analyses. All authors read and approved the final manuscript for publication.

REFERENCES

[1] Furman D, Campisi J, Verdin E, Carrera-Bastos P, Targ S, Franceschi C, Ferrucci L, Gilroy DW, Fasano A, Miller GW, et al. Chronic inflammation in the etiology of disease across the life span. Nat Med 2019; 25(12): 1822-1832. https://doi.org/10.1038/s41591-019-0675-0.

[2] Wautier JL, Wautier MP. Pro- and anti-inflammatory prostaglandins and cytokines in humans: A mini review. Int J Mol Sci 2023; 24(11): 9647. https://doi.org/10.3390/ijms24119647.

[3] Arfeen M, Srivastava A, Srivastava N, Khan RA, Almahmoud SA, Mohammed HA. Design, classification, and adverse effects of NSAIDs: A review on recent advancements. Bioorg Med Chem 2024; 112: 117899. https://doi.org/10.1016/j.bmc.2024.117899.

[4] Khalil NA, Ahmed EM, Tharwat T, Mahmoud Z. NSAIDs between past and present: A long journey towards an ideal COX-2 inhibitor lead. RSC Adv 2024; 14(42): 30647-30661. https://doi.org/10.1039/D4RA04686B.

[5] Domper Arnal MJ, Hijos-Mallada G, Lanas A. Gastrointestinal and cardiovascular adverse events associated with NSAIDs. Expert Opin Drug Saf 2022; 21(3): 373-384. https://doi.org/10.1080/14740338.2021.1965988.

[6] Ghoneim MM, Abdelgawad MA, Elkanzi NAA, Bakr RB. Review of the recent advances of pyrazole derivatives as selective COX-2 inhibitors for treating inflammation. Mol Divers 2025; 29(2): 1789-1820. https://doi.org/10.1007/s11030-024-10906-9.

[7] Chahat, Gupta S, Joshi G, Wahajuddin M, Kumar B. COX-2 inhibitors in inflammation and cancer: Recent developments in medicinal chemistry. Eur J Med Chem 2026; 310: 118781. https://doi.org/10.1016/j.ejmech.2026.118781.

[8] Lai H, Liang Y, Xu J, Guo L, Deng C, Wang X, Zha D. Converting indoprofen to moderate selective COX-2 inhibitors: Design, synthesis and biological evaluation. Bioorg Chem 2025; 162: 108593. https://doi.org/10.1016/j.bioorg.2025.108593.

[9] Elgohary MK, Elkotamy MS, Alkabbani MA, Abdel-Aziz HA. Fenamates and ibuprofen as foundational components in the synthesis of innovative, targeted COX-2 anti-inflammatory drugs, undergoing thorough biopharmacological assessments and in-silico computational studies. Bioorg Chem 2024; 147: 107393. https://doi.org/10.1016/j.bioorg.2024.107393.

[10] Shah M, Parmar R, Patel K, Nagani A. Indole-based COX-2 inhibitors: A decade of advances in inflammation, cancer, and Alzheimer's therapy. Bioorg Chem 2024; 153: 107931. https://doi.org/10.1016/j.bioorg.2024.107931.

[11] Pibiri I. Recent advances: Heterocycles in drugs and drug discovery. Int J Mol Sci 2024; 25(17): 9503. https://doi.org/10.3390/ijms25179503.

[12] Mahmood SA, Mahdi MF, Rauf AMR. A novel series of pyrazole and thiadiazole derivatives bearing nabumetone moiety: Design, molecular docking study, synthesis, characterization, and preliminary pharmacological evaluation. Iraqi J Pharm Sci 2025; 34(1): 85-95. https://doi.org/10.31351/vol34iss1pp85-95.

[13] Wu Z, Chen S, Wang Y, Li F, Xu H, Li M, Zeng Y, Wu Z, Gao Y. Current perspectives and trend of computer-aided drug design: A review and bibliometric analysis. Int J Surg 2024; 110(6): 3848-3878. https://doi.org/10.1097/JS9.0000000000001289.

[14] Hameed TM, Abdulqader KA, Abdulnabi AA, Alawad KM, Hamid AA. Docking, dynamic simulation and ADME studies of new 1,2,3-triazole-based molecules for potential anticancer applications. Trop J Pharm Res 2026; 25(3): 315-328. https://doi.org/10.4314/tjpr.v25i3.4.

[15] Xu S, Hermanson DJ, Banerjee S, Ghebreselasie K, Clayton GM, Garavito RM, Marnett LJ. Oxicams bind in a novel mode to the cyclooxygenase active site via a two-water-mediated hydrogen-bonding network. J Biol Chem 2014; 289(10): 6799-6808. https://doi.org/10.1074/jbc.M113.517987.

[16] Paggi JM, Pandit A, Dror RO. The art and science of molecular docking. Annu Rev Biochem 2024; 93: 389-410. https://doi.org/10.1146/annurev-biochem-030222-120000.

[17] Abraham MJ, Murtola T, Schulz R, Páll S, Smith JC, Hess B, Lindahl E. GROMACS: High performance molecular simulations through multi-level parallelism from laptops to supercomputers. SoftwareX 2015; 1-2: 19-25. https://doi.org/10.1016/j.softx.2015.06.001.

[18] Daina A, Michielin O, Zoete V. SwissADME: A free web tool to evaluate pharmacokinetics, drug-likeness and medicinal chemistry friendliness of small molecules. Sci Rep 2017; 7: 42717. https://doi.org/10.1038/srep42717.

[19] Daina A, Zoete V. A BOILED-Egg to predict gastrointestinal absorption and brain penetration of small molecules. ChemMedChem 2016; 11(11): 1117-1121. https://doi.org/10.1002/cmdc.201600182.

[20] Fu L, Shi S, Yi J, Wang N, He Y, Wu Z, Peng J, Deng Y, Wang W, Wu C, et al. ADMETlab 3.0: An updated comprehensive online ADMET prediction platform enhanced with broader coverage, improved performance, API functionality and decision support. Nucleic Acids Res 2024; 52(W1): W422-W431. https://doi.org/10.1093/nar/gkae236.